Vortex plastic flow, local flux density, magnetization hysteresis loops, and critical current, deep in the Bose-glass and Mott-insulator regimes

C. Reichhardt, C. J. Olson, J. Groth, Stuart Field, and Franco Nori

Department of Physics, The University of Michigan, Ann Arbor, Michigan 48109-1120

We present simulations of flux-gradient-driven superconducting vortices interacting with strong columnar pinning defects as an external field $H(t)$ is quasistatically swept from zero through a matching field B_ϕ. We analyze several measurable quantities, including the local flux density $B(x,y,H(t))$, magnetization $M(H(t))$, critical current $J_c(B(t))$, and the individual vortex flow paths. We find a significant change in the behavior of these quantities as the local flux density crosses B_ϕ, and quantify it for many microscopic pinning parameters. Further, we find that for a given pin density $J_c(B)$ can be enhanced by maximizing the distance between the pins for $B < B_\phi$.

Introduction. Flux pinning by correlated disorder in superconductors has recently been the subject of intense investigations because of its ability to immobilize vortices, reduce dissipation effects, and create high critical currents.[1] In particular, the introduction of correlated disorder by heavy ion irradiation can create columnar defects in which vortices are pinned along their entire length.[2] Such systems are predicted to form a Bose glass at low temperatures when the vortices localize at randomly placed columnar pins.[3,4] The behavior of this state depends on whether the magnetic flux density B is below, equal to, or greater than B_ϕ, the matching field at which the number of flux lines equals the number of columnar pins.[5–7] In addition, an important role is played by the critical state,[8,9] in which a gradient in the flux profile arises as individual vortices enter the sample and become pinned at defects. This gradient determines $J_c(B)$.[1,8,9] Detailed information on the vortex dynamics in the critical state, including *local* and averaged physical quantities, is required to explain the effects induced by the addition of columnar defects. Furthermore, understanding the effect of the spatial distribution of the pinning sites on the Bose glass can facilitate creating samples with optimal pinning to enhance J_c, which is of technological importance. To investigate the *flux-gradient-driven* dynamics of vortices in superconductors with columnar defects, we perform simulations of individual vortices *and* antivortices interacting with strong columnar pinning sites, as an external field $H(t)$ is swept through a complete loop. We monitor distinct changes in relevant physical quantities (e.g., B, M, J_c).

Simulation. We simulate an infinite slab with a magnetic field $\mathbf{H} = H\mathbf{z}$ applied parallel to the surface so that there are no demagnetization effects. We consider rigid vortices and straight columnar pins of uniform strength (all $\|\mathbf{z}$); thus we only need to model a transverse two-dimensional (2D) slice (x-y plane) from the 3D slab. Our results are for a $36\lambda \times 36\lambda$ system with periodic boundary conditions, where λ is the penetration depth. Our superconducting system has a pinned region from $x = 6\lambda$ to $x = 30\lambda$; thus 1/3 of the system is unpinned and 2/3 has randomly placed nonoverlapping parabolic traps with radius $\xi_p = 0.15\lambda$. The flux lines evolve according to a $T = 0$ molecular dynamics algorithm. Thus,

thermal effects are neglected and we consider a situation deep in the Bose glass regime, where the Mott insulator phase should be observable.[3,4,6] Note that pinning due to columnar disorder is much less sensitive to thermal effects than pinning due to point defects. For instance, for $B < B_\phi$ Täuber *et al.*,[4] working with $Bi_2Sr_2CaCu_2O_8$, find that thermal effects on pinning become relevant only for $T_1 \approx 0.9 T_c \approx 78$ K $\approx T_{irrev}$. Therefore, in this case all temperatures $T < T_1$ may be considered low.

We simulate an increasing external field $H(t)$ as described in Refs. 10 and 11, where we quasistatically add flux lines to the unpinned region; these flux lines attain a uniform density n, so that an external applied field H may be defined as $H = n\Phi_0$. As the external field increases, the flux lines—by their own mutual repulsion—are forced into the pinned region where their motion is impeded by the defects. We correctly model the vortex-vortex force by a modified Bessel function $K_1(r/\lambda)$, which falls off exponentially so that a cutoff at 6λ can be safely imposed. The overdamped equation of motion is: $\mathbf{f}_i = \mathbf{f}_i^{vv} + \mathbf{f}_i^{vp} = \eta\mathbf{v}_i$, where the total force $\mathbf{f}_i$ on vortex i (due to other vortices $\mathbf{f}_i^{vv}$, and pinning sites $\mathbf{f}_i^{vp}$) is

$$\mathbf{f}_i = \sum_{j=1}^{N_v} f_0 \, K_1(|\mathbf{r}_i - \mathbf{r}_j|/\lambda) \, \hat{\mathbf{r}}_{ij}$$

$$+ \sum_{k=1}^{N_p} \frac{f_p}{\xi_p} |\mathbf{r}_i - \mathbf{r}_k^{(p)}| \, \Theta((\xi_p - |\mathbf{r}_i - \mathbf{r}_k^{(p)}|)/\lambda) \, \hat{\mathbf{r}}_{ik}.$$

Here Θ is the Heaviside step function, $\mathbf{r}_i$ ($\mathbf{v}_i$) is the location (velocity) of the ith vortex, $\mathbf{r}_k^{(p)}$ is the location of the kth pinning site, ξ_p is the radius of the pinning well, f_p is the maximum pinning force, and we take $\eta = 1$. We measure lengths in units of the penetration depth λ, forces in terms of $f_0 = \Phi_0^2/8\pi^2\lambda^3$ $(= 2\epsilon_0/\lambda)$, energies in units of $\epsilon_0 = (\Phi_0/4\pi\lambda)^2$ $(= f_0\lambda/2)$, and magnetic fields in units of Φ_0/λ^2. The sign of the interaction between vortices is determined by f_v; we take $f_v = +f_0$ for repulsive vortex-vortex interactions and $f_v = -f_0$ for attractive vortex-antivortex interactions. A vortex and antivortex annihilate and are removed from the system if they come within 0.3λ
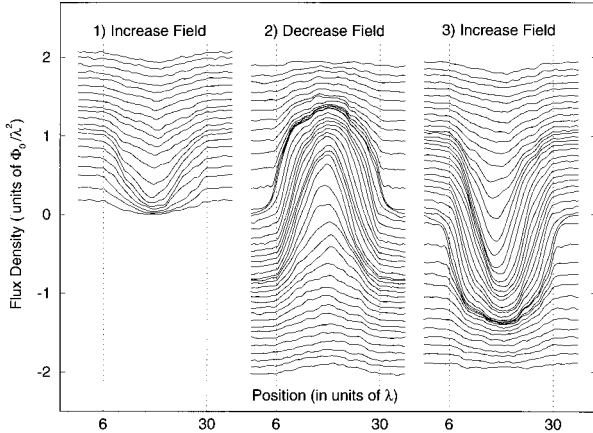
FIG. 1. Magnetic flux density profiles, $B(x,H(t)) = (36\lambda)^{-1}\int_0^{36\lambda} dy B(x,y,H(t))$, for a $36\lambda \times 36\lambda$ system with a $24\lambda \times 36\lambda$ region (the actual sample) containing 864 pinning sites with $f_p = 2.5f_0$, and $\xi_p = 0.15\lambda$. Here $B_\phi = 1.0\ \Phi_0/\lambda^2 = 864\ \Phi_0/(36\lambda \times 24\lambda)$. For the initial ramp-up phase in (1) a total of 2600 vortices are added, so the maximum external field is $2.0\ \Phi_0/\lambda^2 \approx 2600\ \Phi_0/(36\lambda \times 36\lambda)$. In (2) the field is ramped down and then reversed to a final value of $-2.0\ \Phi_0/\lambda^2$. Finally in (3), the field is brought up to $2.0\ \Phi_0/\lambda^2$. A large gradient in B can be seen for $|B| < B_\phi$.

of one another. For columnar pinning the condensation energy is $\epsilon_0 = (\Phi_0/4\pi\lambda)^2$, which can be related to the maximum pinning force f_p to give $f_p/f_0 = \lambda/\xi_p = \lambda/0.15\lambda \approx 7$. However the measurable quantities of the system do not change for pinning forces greater than $2.0f_0$. We systematically vary one parameter such as the density of pins n_p, pinning strength f_p, or the spatial distribution of pinning, while keeping the other parameters fixed. Previous simulations of flux-gradient-driven vortices[10,11] considered situations where $B < B_\phi$ and $f_p/f_0 < 1$ and found a $J_c(H)$ dependence as $1/H$. This corresponds to the experimentally common situation described by the Kim model.[9] However, when we consider very strong columnar pins ($f_p/f_0 > 2.0$) we find a very different behavior.

Flux profiles. From the location of the vortices, we compute their local density $B(x,y,H(t))$ and profile $B(x,H(t))$ inside the sample. Figure 1 shows a typical example of $B(x)$ for a hysteresis loop. When $|B| < B_\phi$, the gradient of the flux profile (i.e., the current J_c) is very large. Above B_ϕ we see an abrupt change in the flux profile to a much shallower slope. As the external field is ramped still higher, the slope of B decreases gradually. These results are very similar to those observed experimentally[7,12] for samples with columnar pins as the local field is increased beyond B_ϕ and

quite different from the ones seen in other types of samples (e.g., Refs. 9, 10, and 11). Such results have been interpreted in terms of a change in the pinning force: when $B < B_\phi$ the vortices are pinned at individual defects, and when $B > B_\phi$ many vortices are pinned at interstitial sites due to the repulsion from the defect-pinned vortices.[5,6,7]

To give a more microscopic idea of the behavior in this system, in Figs. 2(a)–(c) we present snapshots of the positions of the pins and the vortices in an $8\lambda \times 8\lambda$ region of the sample (while the external field is gradually increased). The vortices are entering from the left of the figures and thus there is a flux gradient in the three frames. In Fig. 2(a), most of the vortices are pinned at defects; only two (located near other defect-pinned flux lines) are at interstitial sites. Since most of the vortices at these low fields are trapped by defects, the effective pinning force is very high and hence, as seen in Fig. 1, the flux gradient for low fields is quite steep. In Fig. 2(b), near B_ϕ, a greater fraction of interstitially pinned vortices is present, producing a much lower flux gradient. The fact that unoccupied pins are typically located very close to occupied pins indicates that many unoccupied pins are being "screened" by the vortex repulsion from the occupied pins. Also, because of the flux gradient, there are more interstitially pinned vortices near the left of the figure than the right. Thus, the presence of a flux gradient limits the number of accessible pinning sites, when these sites are randomly distributed. Finally in Fig. 2(c), above B_ϕ, the flux gradient is small and hence the effective pinning force is low. Here a large number of vortices are weakly trapped at interstitial sites and the majority of the defects are now occupied by vortices. In the lower left corner a small domain of triangularly-arranged vortices can be seen—indicating that the vortex-vortex repulsion is starting to dominate over the vortex-pin attraction.

Magnetization loops and critical current. From the microscopic vortex dynamics of individual vortices described above, we can compute macroscopic measurable quantities. In particular, we quantify the vortex behavior described above, as the field is brought through B_ϕ, by measuring $M(H)$ and $J_c(B)$ for samples with different pinning parameters [see Fig. 3]. For instance, the effect of changing the matching field B_ϕ is examined in Figs. 3(a) and (b) by fixing f_p at $2.5f_0$ and changing the pin density n_p. For all the cases we considered, the width of the magnetization curve is much broader when $|B| < B_\phi$, falling off very rapidly when $B > B_\phi$.[7,13] Figure 3 shows the enhancement of $J_c(B)$, for $B < B_\phi$, as the field is swept. We obtain $J_c(B)$ directly from the flux density profiles using Maxwell's equation $dB/dx = \mu_0 J$. For a fixed field H, we average the slope of B over the entire sample. In all cases the enhancement of
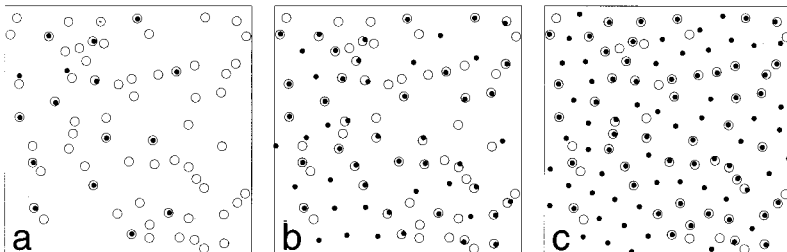

FIG. 2. An $8\lambda \times 8\lambda$ region of the $24\lambda \times 36\lambda$ sample studied in Fig. 1. The vortices enter from the left edge of each frame (which corresponds to the sample edge). Panels (a), (b), and (c) correspond to $B/B_\phi \approx 0.3$, 1.0, and 1.6, respectively, of the ramp up phase in Fig. 1. Pinning sites are indicated by open circles, while the eastbound vortices are shown as filled dots.
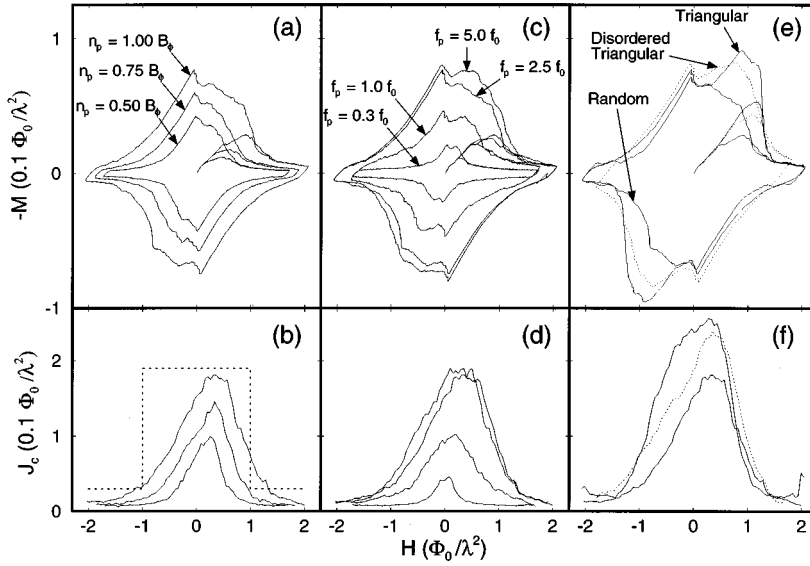
FIG. 3. Magnetization loops (top panels) and the corresponding critical currents (bottom panels) for several samples. The $J_c(B)$s are taken directly from the $B(x)$ during "ramp-down" [e.g., stage (2) in Fig. 1]. In (a) and (b) f_p is held fixed at $2.5f_0$ and the density of pinning sites n_p is varied: $B_\phi/\Phi_0 = 0.50/\lambda^2$, $0.75/\lambda^2$, $1.0/\lambda^2$. In (c) and (d) n_p remains fixed ($B_\phi = 1.0\ \Phi_0/\lambda^2$) and the pinning strength f_p is changed. In (e) and (f) $B_\phi = 1.0\ \Phi_0/\lambda^2$, $f_p = 2.5f_0$, and the location of the pinning sites is varied. (f) shows the significant *enhancement* of $J_c(B)$ that results from defects placed in a regular triangular array, as opposed to random placement. These results show that even a distorted triangular array of pinning sites significantly enhances $J_c(B)$ over the case with a random location of pinning sites.

$J_c(B)$ is restricted to $|B| < B_\phi$. This is very similar to the experimental results seen in Ref. 12 at low T, where $J_c(B)$ was also obtained directly from the flux gradient. It can also be seen from Fig. 3 that J_c has a definite dependence on B, which is different from the steplike two-current model suggested in Refs. 6 and 7 [indicated by a dashed line in Fig. 3(b)].

We next examine the effect of varying the pinning force from $f_p = 0.3f_0$ to $f_p = 5.0f_0$ [see Figs. 3(c) and (d)]. There is little change in $M(H)$ and $J_c(B)$ as the pinning force is increased from $f_p = 2.5f_0$ to $f_p = 5.0f_0$. This reflects the fact that once vortices are trapped strongly enough, so that they cannot be unpinned, any further increase in the pinning strength does not significantly affect $M(H)$ and $J_c(B)$. As the pinning force is decreased in Fig. 3(c), the width of the magnetization loop narrows. A sudden drop in $M(H)$ near B_ϕ is no longer observed when the pinning force from the individual defects becomes on the order of the interstitial pinning force (when $f_p \sim f_0/2$). This behavior is emphasized in Fig. 3(d) (where $B_\phi = \Phi_0/\lambda^2$) for $J_c(B)$. At the lowest pinning strengths [bottom curve in Fig. 3(d)], only a small increase in $J_c(B)$ can be seen when $|B| < B_\phi/3$, and not when $|B| < B_\phi$ as in the strongly pinned cases (top two curves, where $f_p \gtrsim 2.0f_0$). These results are very similar to those seen in Ref. 12 when the temperature was raised, which reduces the effective pinning strength.

The theory of a Mott insulator phase in the Bose glass[3] leads one to expect an enhancement in $J_c(B)$ at B_ϕ. At this field the vortices become strongly localized at the pinning sites, due to the repulsion of the other vortices, and produce a Meissner-like phase which prevents increased flux penetration over a range of field. However, we do *not* observe any particular enhancement of J_c at $B = B_\phi$. This is due to the combined effects of *both* the critical state, which prevents a uniform field in the sample, and the randomness in the spatial distribution of defects, which prevents all the pins from being occupied due to the "screening" effects induced by closely spaced pinning sites, as discussed above. We point out that near B_ϕ there can still be a decrease in the magnetization relaxation rate since it depends on thermal activation and tunneling.

We can significantly reduce screening effects (due to closely spaced defects) by changing the spatial arrangement of the pinning sites, thus enhancing J_c. Figures 3(e) and (f) present $M(H)$ and $J_c(B)$ for three systems with pinning sites which are (1) randomly located, (2) placed in a triangular lattice (see, e.g., Ref. 14), and (3) randomly displaced, up to 0.25λ from a triangular lattice. All three systems have $B_\phi = \Phi_0/\lambda^2$ and $f_p = 2.5f_0$. For fields less than B_ϕ, the width of $M(H)$ and $J_c(B)$ for the triangular pinning is nearly twice that for the random case. The asymmetry in $M(H)$ and $J_c(B)$ is much more pronounced when pins are placed in a triangular lattice. For this case, there is also a very sharp drop in $M(H)$ just past B_ϕ, very similar to that observed in Ref. 14, since here the distinction between vortex pinning at defects and interstitial pinning is much better defined. This result is very important since it indicates that substantial increases in the critical current for fields less then B_ϕ can be achieved by evenly spacing the pins. In this case, $M(H)$ and $J_c(B)$ are enhanced because all the pins are accessible to the vortices, as opposed to the random case where it is difficult for vortices to reach closely spaced defects. Moreover, in the system with triangular pinning, trapped vortices are better localized at the defects due to the interactions with other pinned vortices (since an additional energy minima is present when the vortices are in a favorable lattice configuration). This indicates that the Mott insulator phase is more accessible in a triangular array of pinning sites than in a Bose glass with randomly located defects. In the "disordered triangular" case [see Fig. 3(e)] where the pinning sites are randomly displaced (up to 0.25λ) from the triangular sites, there is still a clear enhancement of $J_c(B)$; however, it is much smaller than in the ordered triangular pinning array.

Vortex plastic flow. To investigate the dynamics of the flux-gradient-driven vortices near B_ϕ and higher fields, we present in Figs. 4(a) and (b) the trajectories of the vortices for a system with (a) strong pinning, $f_p = 2.5f_0$, and with (b) weaker pinning, $f_p = 0.3f_0$, both with $B_\phi = 1.0\ \Phi_0/\lambda^2$. For both panels the external field H is increased from $0.9\ \Phi_0/\lambda^2$ to $1.4\ \Phi_0/\lambda^2$. In (a) the moving vortices follow specific winding channels indicative of *plastic flow* of interstitial vortices around domains of flux lines which are
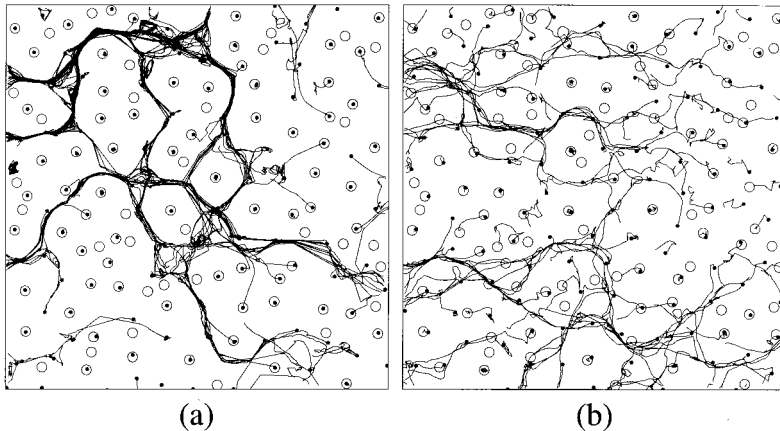
FIG. 4. (a) and (b) show the trajectories of eastbound vortices while the external field is raised from $0.95\Phi_0/\lambda^2$ to $1.4\Phi_0/\lambda^2$. (a) A $10\lambda \times 10\lambda$ region of the sample used in Fig. 1. The strength of the pinning force, f_p, is $2.5f_0$, for the strong-pinning case (a), and $0.3f_0$, for the weak-pinning case (b). In (a) the vortex transport is characterized by vortex trails of *interstitial* vortices which move around regions with flux lines that are strongly pinned at defects. In (b) vortex transport proceeds in a different manner; pin-to-pin vortex motion, as well as interstitial, is possible and the previously narrow vortex trails become considerably broader.

strongly pinned at defects. These ''vortex rivers'' often develop well-defined tight *bottlenecks* as well as much broader ''vortex streets'' with several lanes. At the top left side of Fig. 4(a), two bottlenecks can be seen. Each of these ''interstitial vortex paths'' is located between flux lines that are strongly pinned at defects, indicating that the interstitial vortices are flowing through the energy minima created by the strongly pinned flux lines. These interstitial-vortex-channels form for both the entrance and exit of vortices and are a general feature of all simulations with randomly placed strong pinning sites. It is interesting to note that although a large number of vortices are clearly immobile at the defects, J_c is quite low for this region of $B > B_\phi$ indicating that the channels are acting as *weak links*. In Fig. 3(b) with $f_p = 0.3f_0$ we see a much different behavior with broader channels. Further, it can be observed from the lines that cross through pinning sites that vortices can become unpinned since the pinning force is on the order of the interstitial pinning. Thus vortex motion consists of both interstitial trajectories and also pin-to-pin motion.

Conclusions. Our simulations of flux-gradient-driven rigid vortices interacting with columnar pinning sites are consistent with recent experiments[7,12,13] which indicate that a sharp change in the magnetic flux gradient occurs above B_ϕ. Our results *quantitatively* predict how J_c varies with field and pinning parameters (e.g., strength and location). Moreover, we can monitor the spatio-temporal dynamics of vortices as the pinning mechanism evolves from strong columnar pinning (for $B < B_\phi$) to weaker interstitial pinning (for $B > B_\phi$). In particular, we quantify the enhancement of J_c, when $B < B_\phi$, by varying the spatial arrangements of the pinning sites. When the pinning strength of the columnar defects becomes on the order of the interstitial pinning strength, this sharp transition in J_c is greatly reduced. We compute the spatiotemporal dynamics of vortices and show that for strongly pinned samples the vortex transport is dominated by the plastic flow of interstitially pinned vortices around regions of flux lines strongly pinned at defects. In the weaker pinning samples, vortices can jump from defect to defect site. Finally, M and J_c can be considerably enhanced by placing the defects on a regular triangular lattice, for a given pin density, so that all pins are equally accessible, thus preventing the screening of closely-spaced defects occurring in a random distribution.

[1] The literature on vortices is vast and we do not attempt a review here. For recent reviews, and an extensive list of references, see, e.g., G. Blatter *et al.*, Rev. Mod. Phys. **66**, 1125 (1994); E.H. Brandt (unpublished).

[2] See, e.g., L. Civale *et al.*, Phys. Rev. Lett. **67**, 648 (1991); W. Gerhäuser *et al.*, *ibid.* **68**, 879 (1992); R.C. Budhani *et al.*, *ibid.* **69**, 3816 (1992); M. Konczykowski *et al.*, Phys. Rev. B **44**, 7167 (1991).

[3] D.R. Nelson and V. M. Vinokur, Phys. Rev. B **48**, 13 060 (1993).

[4] U.C. Täuber *et al.*, Phys. Rev. Lett. **74**, 5132 (1995); H. Dai *et al.*, Science **265**, 1552 (1994); U.C. Täuber and D.R. Nelson, Phys. Rev. B **52**, 16 106 (1995).

[5] I.B. Khalfin and B. Ya. Shapiro, Physica C **207**, 359 (1993).

[6] L. Radzihovsky, Phys. Rev. Lett. **74**, 4919 (1995); **74**, 4923 (1995).

[7] K.M. Beauchamp *et al.*, Phys. Rev. B **52**, 13 025 (1995).

[8] C.P. Bean, Rev. Mod. Phys. **36**, 31 (1964).

[9] Y.B. Kim *et al.*, Rev. Mod. Phys. **36**, 43 (1964).

[10] R.A. Richardson, O. Pla, and F. Nori, Phys. Rev. Lett. **72**, 1268 (1994).

[11] C. Reichhardt, C.J. Olson, J. Groth, S. Field, and F. Nori, Phys. Rev. B **52**, 10 411 (1995).

[12] M. Konczykowski *et al.*, Physica C **235-240**, 2965 (1994).

[13] K.M. Beauchamp *et al.*, Phys. Rev. Lett. **75**, 3942 (1995).

[14] M. Baert *et al.*, Phys. Rev. Lett. **74**, 3269 (1995).